Summation of two-pion inserts to the σ-meson propagator and nucleon forces*

Earle L. Lomon

Laboratory for Nuclear Science and Department of Physics, Massachusetts Institute of Technology, Cambridge, Massachusetts 02139

(Received 23 February 1976)

Each pion-pair insert into a σ-meson propagator leads to a factorizable contribution, a function of the magnitude of the σ-meson four-momentum. The sum of the resulting geometric series produces a modified propagator with a mass shift and a width which are determined by the physical mass and decay rate of the σ meson. The modified propagator is used to calculate the contribution of all nucleon-nucleon scattering diagrams in which the nucleons can be separated by cutting only a σ-meson line. This replaces the treatment of F. Partovi and E. L. Lomon in which the effect of the σ-meson width was approximated by averaging the potential obtained from an unmodified propagator over the σ-meson mass distribution. The new potential, when the general chiral constraint is imposed on the coupling constants, is small, in spite of large coupling strengths, due to cancellations between terms. It is similar to the previous approximate result and is less sensitive to the σ-meson width. The size of the potential is reasonable for widths greater than 300 MeV. As before, the Weinberg-model prediction of a σ meson which has a ρ-meson mass and a width of 620 MeV leads to the best cancellation of nucleon-pair terms away from zero four-momentum transfer. The addition of this contribution to the theoretical potential of M. Hossein Partovi and E. L. Lomon tends to decrease the agreement with several realistic potentials. The size of the σ-meson-exchange contribution is decreased if the σ-meson width is increased; but neglecting exchange contributions a zero-isospin two-pion bound state also arises.

I. INTRODUCTION

The use of quantum relativistic field theory to calculate fundamental particle processes is complicated by radiative corrections to vertex functions [Figs. 1(a), 1(b), and 1(c)] and propagators [Figs 1(d) and 1(e)]. One-pion exchange (the two nucleons are separated on cutting a single pion line) will dominate the nucleon-nucleon force at low momentum transfer over all other single-particle and multiparticle exchanges. However, radiative corrections such as those shown in Figs. 1(a), 1(c), and 1(d) contribute strongly in this kinematical range and must be included with the simple one-pion exchange. Fortunately, in this case of one-pion exchange all possible vertex and propagator inserts have much higher masses than the pion [$M_\sigma+\mu$ in Fig. 1(a) and $2M$ in Figs. 1(c) and 1(d); we use μ and M for the pion and nucleon masses, respectively]. This means that the radi-

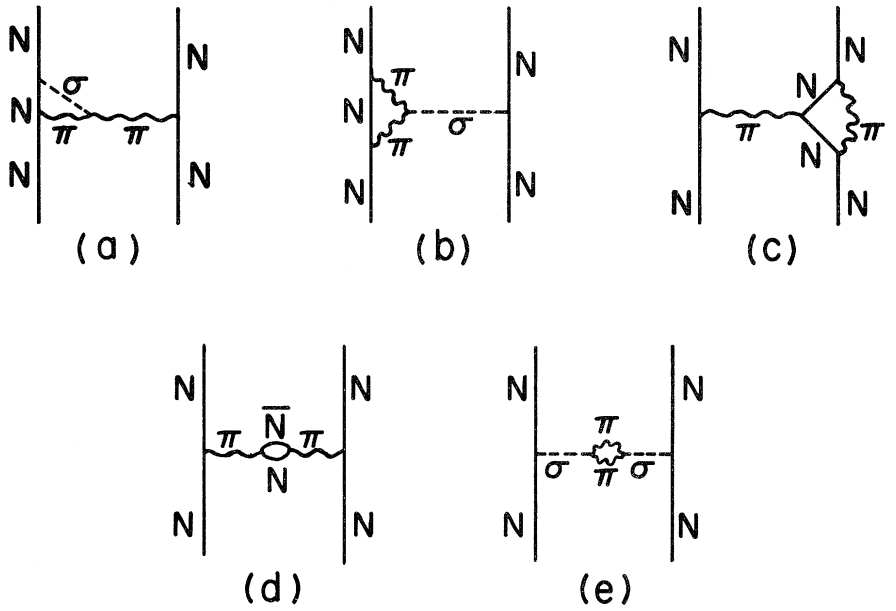

FIG. 1. Representative radiative corrections to one-pion and one-σ-meson exchange contributions to the nucleon-nucleon interaction.

ative corrections can be approximated as independent of q (nucleon momentum transfer) and are therefore absorbed into the renormalized $\pi N\bar{N}$ coupling constant and pion mass, which are given by the physical values.

In many important cases radiative corrections may be taken into account to a good approximation as in the above case. In other cases, such as that of πN scattering (Fig. 2), the sum of all radiative corrections that overlap two of the elementary vertices [Fig. 2(f) is the simplest example] is largely absorbed into resonances (nucleon isobars in the example shown). These isobars can then be treated as elementary particles to a good approximation.[1] Resonance masses and coupling constants can be obtained from high-energy-production experiments.

There are cases, however, in which radiative corrections cannot be treated to good approximation by q-independent constants. Figures 1(b), 1(e), 2(c), 2(d), and 2(e) are examples. The σ meson decays into two pions whose mass is considerably less than M_σ. The resulting vertex and propagator radiative corrections are strongly q-dependent and are not well accounted for by the coupling and mass-renormalization constants determined at $q=0$ and $q=M_\sigma$, respectively ($\hbar=C=1$ in the units of this paper). Because of the strength of the $\sigma\pi\pi$ coupling (the large width of the σ meson) this q-dependent correction is large. The effects must be treated to all orders.

F. Partovi and E. L. Lomon[2] have previously derived the exact q dependence of the vertex corrections [Figs. 1(b) and 2(c)] and applied the results to the nucleon-nucleon force. In Ref. 2 (hereafter referred to as FPL) the effect of the sum of all pion-bubble inserts on the σ-meson propagator as in Figs. 1(e) and 3 was approximated by averaging the σ-exchange potential over the Breit-Wigner mass distribution corresponding to a σ meson. In this paper we derive the exact q dependence of the σ-meson peopagator summed over all pion-bubble inserts (Fig. 3). This enables the exact treatment of all σ-exchange contributions to the nucleon-nucleon force.

There is no double counting of the σ exchange with two-pion-exchange terms if the σ meson is treated as an elementary particle in the Lagrangian of the system. The modified σ-meson propagator may be used to replace the sum in Fig. 3 in any Feynman diagram. Here we apply it only to nucleon-nucleon scattering. A similar modification may be made for other bubble inserts on the propagators of other particles, for instance two-pion bubbles on the ρ-meson propagator. The effect of the latter will be relatively small because of the small ρ-meson width.

In Sec. II the modified propagator will be obtained and related to the physical mass and to the requirements of the chiral (soft-pion) conditions. The application of these results to the nucleon-nucleon force will be treated in Sec. IV,

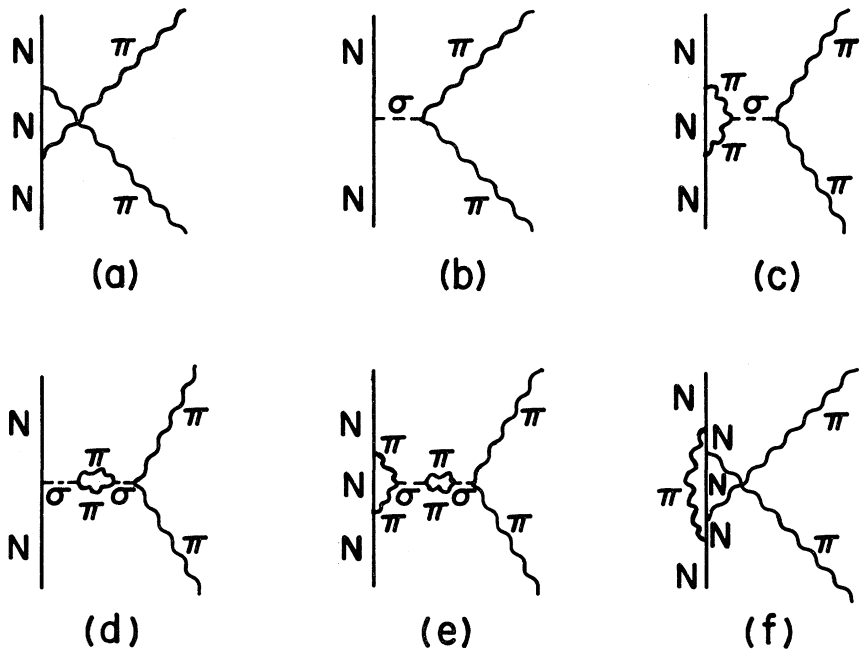

FIG. 2. Representative radiative corrections to nucleon and one-σ-meson exchange contributions to the pion-nucleon interaction.

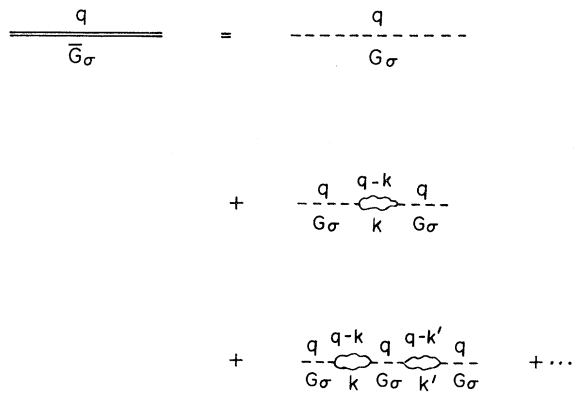

FIG. 3. The modified σ-meson propagator $\bar{G}_\sigma$ composed of any number of pion "bubbles" inserted into the bare σ-meson propagator G_σ. See Eq. (11).

after the general approach to the nucleon force calculation has been reviewed in Sec. III.

II. TWO-PION-BUBBLE MODIFICATION OF THE σ-MESON PROPAGATOR

As indicated symbolically in Fig. 3, the modified σ-meson propagator is

$$\begin{aligned}\bar{G}_\sigma(q^2) &= G_\sigma(q^2) + G_\sigma(q^2) I_B(q^2) G_\sigma(q^2) \\ &\quad + G_\sigma(q^2) I_B(q^2) G_\sigma(q^2) I_B(q^2) G_\sigma(q^2) + \cdots \\ &= G_\sigma(q^2)[1 - I_B(q^2) G_\sigma(q^2)]^{-1} \\ &= [G_\sigma^{-1}(q^2) - I_B(q^2)]^{-1}, \end{aligned} \tag{1}$$

where

$$G_\sigma^{-1}(q^2) = q^2 - (M_\sigma^0)^2, \tag{2}$$

M_σ^0 is the bare mass of the σ meson, and the two-pion-bubble loop integral is

$$I_B(q^2) = i\lambda_B \int d^4k (k^2 - \mu^2 + i\epsilon)^{-1} \times [(q-k)^2 - \mu^2 + i\epsilon]^{-1} \tag{3}$$

with

$$\lambda_B = 6(2\pi)^{-4} g_{\sigma\pi}{}^2. \tag{4}$$

The constants are appropriate for $\sigma\vec{\pi}\cdot\vec{\pi}$ coupling of charge-symmetric pions to the σ meson. Using the usual Feynman technique Eq. (3) becomes

$$\begin{aligned} I_B(q^2) &= i\lambda_B \int d^4k \int_0^1 dz \{(k^2 - \mu^2 + i\epsilon)z + [(q-k)^2 - \mu^2 + i\epsilon](1-z)\}^{-2} \\ &= -2\pi^2 \lambda_B \int_0^1 dz \int_0^\infty k^3 [k^2 - m(q^2) - i\epsilon]^{-2} dk, \end{aligned} \tag{5}$$

with

$$m(q^2) = q^2(z - z^2) - \mu^2.$$

$\mathrm{Re} I_B(q^2)$ is logarithmically divergent. This divergence will be absorbed into the renormalization of M_σ^0 [Eqs. (1) and (2)], as specified later. At this point we proceed with an explicity limiting procedure for $k^2 \to \infty$. Integrating Eq. (5), we obtain

$$I_B(q^2) = \lim_{\Lambda = \infty} -\pi^2 \lambda_B \int_0^1 dz \left(\ln \left| \frac{\Lambda - m(q^2)}{m(q^2)} \right| - 1 + i\pi\Theta[m(q^2)] \right). \tag{6}$$

It is convenient to subtract at $q^2 = 0$

$$\bar{I}_B(q^2) \equiv I_B(q^2) - I_B(0). \tag{7}$$

Note that $I_B(0)$ is real and divergent, but $\bar{I}_B(q^2)$ is finite. From Eq. (6)

$$\bar{I}_B(q^2) = \pi^2 \lambda_B \int_0^1 dz \{ \ln|1 - q^2 \mu^{-2}(z - z^2)| - i\pi\Theta[q^2(z - z^2) - \mu^2] \}. \tag{8}$$

Equation (8) is analytically integrable. When $q^2 \geq 4\mu^2$ or $q^2 \leq 0$

$$\begin{aligned} \bar{I}_B(q^2) &= \pi^2 \lambda_B \{ -2 + (1 + |1 - 4q^{-2}\mu^2|^{1/2}) \ln[|1 - q^2(2\mu)^{-2}|^{1/2} + |q|(2\mu)^{-1}] \\ &\quad + (1 - |1 - 4q^{-2}\mu^2|^{1/2}) \ln|[|1 - q^2(2\mu)^{-2}|^{1/2} - |q|(2\mu)^{-1}]| \} \\ &\quad - i\pi^3 \lambda_B |1 - 4q^{-2}\mu^2|^{1/2} \Theta(q^2 - 4\mu^2). \end{aligned} \tag{9a}$$

When $0 \leq q^2 \leq 4\mu^2$

$$\bar{I}_B(q^2) = \pi^2 \lambda_B [-2 + 2(4q^{-2}\mu^2 - 1)^{1/2} \tan^{-1}(4q^{-2}\mu^2 - 1)^{-1/2}]. \tag{9b}$$

The following limits are of interest:

$$\bar{I}_B(q^2) \to -\tfrac{1}{6}\pi^2\lambda_B\mu^{-2}q^2 \quad \text{for } |q^2| \ll 4\mu^2, \tag{10a}$$

$$\bar{I}_B(q^2) \to 2\pi^2\lambda_B \ln|\mu^{-1}q| \quad \text{for } |q^2| \gg 4\mu^2, \tag{10b}$$

and

$$\bar{I}_B(4\mu^2) = -2\pi^2\lambda_B. \tag{10c}$$

From Eqs. (1), (2), and (7) we have the modified propagator

$$\begin{aligned}\bar{G}_\sigma^{-1}(q^2) &= q^2 - (M_\sigma^0)^2 - \bar{I}_B(q^2) - I_B(0) \\ &= q^2 - M_\sigma^2 - \bar{I}_B(q^2) - [I_B(0) - \mathrm{Re}I_B(M_\sigma^2)] \\ &= q^2 - M_\sigma^2 - \bar{I}_B(q^2) + \mathrm{Re}\bar{I}_B(M_\sigma^2),\end{aligned} \tag{11}$$

where

$$M_\sigma^2 \equiv (M_\sigma^0)^2 + \mathrm{Re}I_B(M_\sigma^2) \tag{12}$$

is defined by the observable mass, i.e., the peak of the $\pi\pi$ resonance. The divergence $\mathrm{Re}I_B(M_\sigma^2)$ is canceled by the divergence in the square of the bare σ-meson mass $(M_\sigma^0)^2$. Every term is finite in the last line of Eq. (11). Equation (11) displays the structure of a resonance with mass M_σ because

$$\mathrm{Re}\bar{G}_\sigma^{-1}(q^2) = q^2 - M_\sigma^2 - \mathrm{Re}[\bar{I}_B(q^2) - \bar{I}_B(M_\sigma^2)] \tag{13}$$

vanishes at $q^2 = M_\sigma^2$. The width is determined by Eq. (9a);

$$\begin{aligned}M_\sigma\Gamma_\sigma &\equiv \mathrm{Im}\bar{G}_\sigma^{-1}(M_\sigma^2) \\ &= -\mathrm{Im}\bar{I}_B(M_\sigma^2) \\ &= \pi^3\lambda_B(1 - 4\mu^2M_\sigma^{-2})^{1/2}.\end{aligned} \tag{14}$$

Note also that $\mathrm{Im}\bar{G}_\sigma^{-1}(M_\sigma^2)$ has the correct threshold behavior for an S-state resonance, vanishing at $q = 4\mu$ as $(q^2 - 4\mu^2)^{1/2}$. The simple Breit-Wigner structure of the resonance is modified by the branch points of $\mathrm{Re}I_B(q^2)$ at $q = 2\mu$, $\sqrt{2}\mu$, and ∞.

The modified propagator [Eq. (11)] develops a pole when $\bar{G}_\sigma^{-1}(q^2) = 0$. For real values of q^2 this can only occur if $q^2 < 4\mu^2$, because otherwise $\bar{I}_B(q^2)$ is complex [see Eq. (9a)]. Using the limits of Eqs. (10) and derivatives of Eqs. (9) it can be established that $\bar{I}_B(q^2)$ is monotonically decreasing for $-\infty < q^2 < 4\mu^2$. Also it can be seen from Eqs. (4), (8), and (13) that $\bar{I}_B(q^2)$ is proportional to Γ_σ. For a given M_σ there is then a critical value of Γ_σ at which a pole in $\bar{G}_\sigma(q^2)$ occurs at $q^2 = 4\mu^2$, and larger values of Γ_σ will bring the pole, q_p^2, of $\bar{G}_\sigma(q^2)$ to smaller values of q^2. When $0 < q_p^2 < 4\mu^2$ the pole in the propagator implies a bound pion-pion state. If $q_p^2 < 0$ finite results are obtained, but the pion-scattering prediction would strongly differ from that obtained from the resonance pole alone. We shall therefore assume that $\Gamma_\sigma < \Gamma_\sigma^{\mathrm{crit}}$, as determined by the vanishing of Eq. (11);

$$\begin{aligned}\mathrm{Re}\bar{I}_B^{\mathrm{crit}}(M_\sigma^2) &\equiv \Gamma_\sigma^{\mathrm{crit}}[\Gamma_\sigma^{-1}\mathrm{Re}\bar{I}_B(M_\sigma^2)] \\ &= M_\sigma^2 - [q^2 - \bar{I}_B(q^2)]_{q^2 = 4\mu^2} \\ &= M_\sigma^2 - (4\mu^2 + 2\pi^2\lambda_B),\end{aligned} \tag{15}$$

where $\Gamma_\sigma^{-1}\mathrm{Re}\bar{I}_B(M_\sigma^2)$ is independent of the choice of Γ_σ and λ_B depends linearly on $\Gamma_\sigma^{\mathrm{crit}}$ through Eq. (14).

A complex pole of $\bar{G}_\sigma(q^2)$ corresponds to the Breit-Wigner-type resonance at $q^2 = M_\sigma^2$. The pole can be found numerically, but a good approximation to the position of the pole can be found by using the fact that $q^2 - M_\sigma^2$ is rapidly varying for q^2 near M_σ in Eq. (11). Because of that we can set

$$\mathrm{Re}\bar{I}_B(q^2) - \mathrm{Re}\bar{I}_B(M_\sigma^2) \approx 0 \tag{16a}$$

and [see Eq. (14)]

$$\mathrm{Im}I_B(q^2) \approx -M_\sigma\Gamma_\sigma \quad \text{when } q^2 \text{ is near } M_\sigma^2, \tag{16b}$$

which lead to the simplified relativistic Breit-Wigner form

$$\bar{G}_\sigma(q^2) \approx (q^2 - M_\sigma^2 + iM_\sigma\Gamma_\sigma)^{-1} \tag{17}$$

for which the pole q_p^2 is given by

$$\mathrm{Re}q_p = 2^{-1/2}M_\sigma[1 + (1 + M_\sigma^{-1}\Gamma_\sigma)^{1/2}]^{1/2} \tag{18a}$$

and

$$\mathrm{Im}q_p = -\tfrac{1}{2}M_\sigma[\mathrm{Re}q_p]^{-1}\Gamma_\sigma. \tag{18b}$$

Note that $\mathrm{Re}q_p > M_\sigma$, so that the pole is distant from the branch points, which makes Eq. (17) a good starting point for an iterative solution of the resonance pole of $\bar{G}_\sigma(q^2)$.

In Fig. 4 the curve of $|\bar{G}_\sigma(q^2)|^2$ given by Eq. (11) is compared with the result of the relativistic Breit-Wigner form that includes the threshold dependence [instead of the simplified Eq. (17) form], given by

$$\begin{aligned}G_{\mathrm{BW}}^{-1}(q^2) = q^2 - M_\sigma^2 + i\Gamma_\sigma M_\sigma^2 q^{-1}(q^2 - 4\mu^2)^{1/2} \\ \times (M_\sigma^2 - 4\mu^2)^{-1/2}\Theta(q^2 - 4\mu^2).\end{aligned} \tag{19}$$

The values $M_\sigma = 765$ MeV and $\Gamma_\sigma = 620$ MeV are used.

The curves are quantitatively alike in the vicinity of the resonance peak but are very different elsewhere, although they have similar structure at the two-pion threshold. The exact modified propagator given by Eq. (11) does differ substantially from that given by Eq. (19) in the region $-2M_\sigma^2 < q^2 < 0$ which contributes most to the value of a σ-exchange potential at $r > M_\sigma^{-1}$.

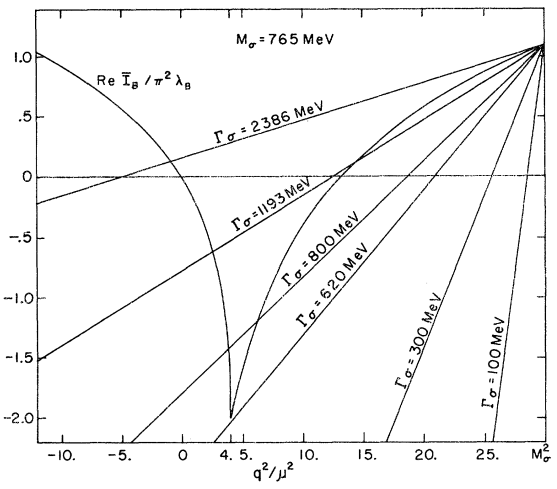

FIG. 4. The linear and nonlinear terms of $\bar{G}_\sigma^{-1}(q^2)$ [Eq. (11)]: The straight lines represent

$$(\pi^2\lambda_B)^{-1}\,[q^2 - M_\sigma{}^2 + \mathrm{Re}\bar{I}(M_\sigma{}^2)]$$

for $M_\sigma = 765$ MeV and the several indicated values of Γ_σ. The slopes depend on Γ_σ through λ_B [Eqs. (4) and (14)], but all the lines cross at $q^2 = M_\sigma{}^2$, because $(\pi^2\lambda_B)^{-1}\mathrm{Re}\bar{I}(M_\sigma{}^2)$ is independent of Γ_σ. Similarly, the curve $(\pi^2\lambda_B)^{-1}\mathrm{Re}\bar{I}_B(q^2)$ is independent of Γ_σ. $\mathrm{Re}\bar{G}^{-1}(q^2)$ vanishes at the values of q^2 where the straight line intesects the curve with the cusp. When this intersection occurs for $q^2 < 4\mu^2$, where $\bar{G}_\sigma$ is real, a real pole of $\bar{G}_\sigma$ results.

The values of M_σ and Γ_σ used in Fig. 5 are those that correspond to the Weinberg π, σ, ρ, A meson model[3] (with the Goldberger-Treiman value $g_A/g_V = 1.37$) and also correspond to the results of the pion-production data analysis of Kim and Bander.[4] For this case Eq. (18) gives $\mathrm{Re}(q_p) \approx 818$ MeV. If instead we use $\Gamma_\sigma = 1193$ MeV (corresponding to the Gell-Mann–Lévy model[5] with $g_A/g_V = 1.37$ or to the Weinberg model[3] with $g_A/g_V = 1$) we obtain $\mathrm{Re}(q_p) = 912$ MeV. The latter is close to the pole analysis of the data by Hyams *et al.*[6] for which $q_p = 1049$ MeV. Another analysis by Basdevant *et al.*[7] suggests $M_\sigma = 500$ MeV and $\Gamma_\sigma = 700$–1200 MeV.

Although M_σ and Γ_σ are not uniquely defined by the high-energy data or by chiral models, we will see that the predictions for nucleon-nucleon forces are reasonbale for the wide range of cases described above. A better determination of M_σ and Γ_σ may come first either from high-energy production data or from a comparison with nucleon-nucleon data after an adequate specification of the rest of the medium-range theoretical potential.

To complete our preparation for examining nucleon forces we need to calculate the radiative corrections to the $\sigma N\bar{N}$ vertex, including the effect of the modified propagator, and determine the consequent renormalization of the $\sigma N\bar{N}$ coupling constant. Figure 6 illustrates the series

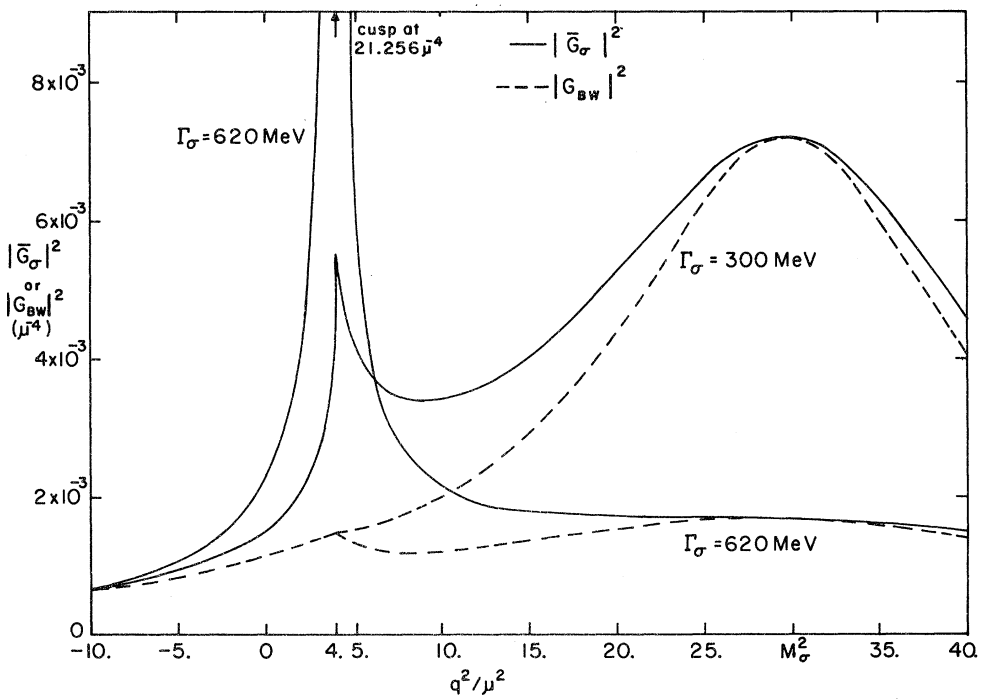

FIG. 5. Comparison of the propagator $|\bar{G}_\sigma|^2$, which includes the complete pion "bubble sum," with the Breit-Wigner form for s-state resonances $|G_{BW}|^2$.

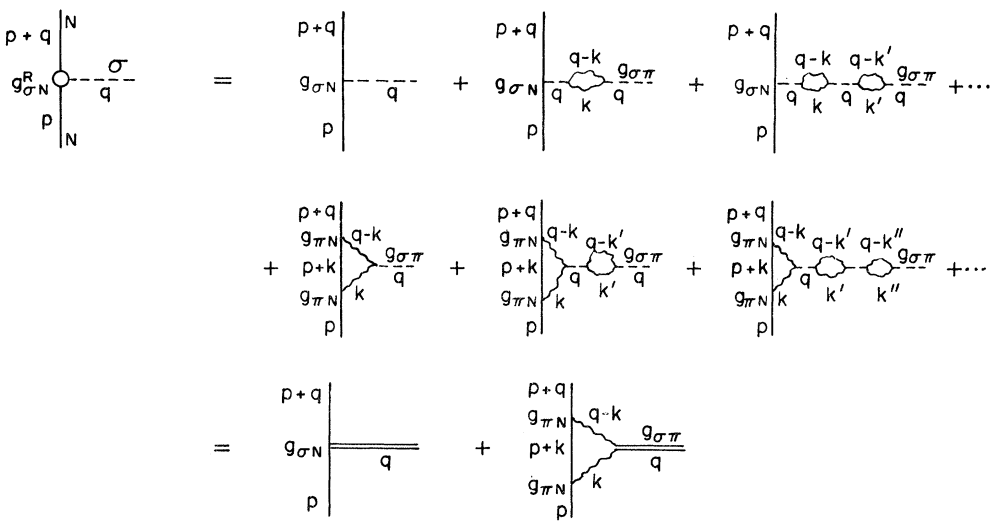

FIG. 6. The exact $\sigma N\bar{N}$ vertex function expanded into all terms arising from the decay of the σ meson into two pions. Corrections to $\sigma N\bar{N}$ or $\pi N\bar{N}$ vertices arising from mesons which are emitted and absorbed on the nucleon line are included in the definition of the coupling constants $g_{\sigma N}$ and $g_{\pi N}$. The two infinite series are exactly summed by the two modified-σ-propagator diagrams. See Eq. (20).

of Feynman diagrams that contribute to the vertex function, and the two diagrams with modified σ-meson propagators that sum up the whole series.

The momentum-transfer dependence of the $\pi\pi N$ loop is given by the function $R(q^2)$ defined by Eq. (37) of FPL, and the q^2 dependence of the modified propagator is given by Eq. (11) of this article. To define the renormalized coupling constant $g^R_{\sigma N}$ in relation to the coupling constant $g_{\sigma N}$ which does not take into account the radiative corrections of Fig. 6 [but takes into account others analogous to Fig. 1(a)] we evaluate Fig. 6 for $q^2=0$ using the modified-propagator diagrams. This is equivalent to Eq. (3) of FPL with a modification of the propagator on the right-hand side:

$$M_\sigma{}^{-2} g^R_{\sigma N} = [M_\sigma{}^2 - \mathrm{Re}\bar{I}_B(M_\sigma{}^2)]^{-1} \times [g_{\sigma N} - 6(4\pi)^{-2} g_{\pi N}{}^2 g_{\sigma\pi} MR(0)], \tag{20}$$

where

$$MR(0) \equiv \mathcal{J}(M) = -M^{-1} + M^{-3}(M^2-\mu^2)\ln(M/\mu) + \mu M^{-3}(4M^2-\mu^2)^{-1/2}(3M^2-\mu^2)\cos(\tfrac{1}{2}\mu/M). \tag{21}$$

The resulting $g^R_{\sigma N}$ is the appropriate coupling constant to use in the chiral condition [Eq. (1) of FPL] which requires that the sum of pion-nucleon scattering amplitudes [Figs. 2(a)–2(e) and 6] vanishes in the limit of zero four-momentum transfer $q=0$; viz.,

$$g^R_{\sigma N} g_{\sigma\pi} = \tfrac{1}{2} M^{-1}(M_\sigma{}^2 - \mu^2) g_{\pi N}{}^2. \tag{22}$$

Equations (4), (8), (10), (13), (15), (20), and (22) define all the quantities needed for application to nucleon and pion scattering problems.

If in addition we impose the constraints of the Weinberg model[3] that $g^R_{\sigma N} = \sqrt{2}(g_A/g_V) g_{\pi N}$ and $M_\sigma = 765$ MeV there are no free parameters [except those due to the ambiguity of the appropriate choice of (g_A/g_V)]. If the Gell-Mann–Lévy model[5] is imposed, then $g^R_{\sigma N} = (g_A/g_V) g_{\pi N}$ but M_σ is a free parameter.

III. ROLE OF THE RADIATIVE CORRECTIONS AND THE σ MESON IN THE NUCLEON FORCE PROBLEM

The longest-range interactions between particles are caused by the exchange of the lighest particles or groups of particles. This implies that detailed calculation of the interaction is easiest at the longest range where one-particle exchange suffices and becomes successively more complicated at shorter ranges. The manifestation of this effect in dispersion relations is the relative simplicity of the singularities due to one- or two-particle exchange; in field theory it is the small number of required integrations in the Feynman amplitudes and the small number of diagrams.

In configuration space the range dependence of an interaction is exponential, so that contributions which differ discretely in the mass exchanged have rather well-separated domains. Thus the configuration-space description of interactions has the advantage that the longer-range part, calculable from theory, is separated in a comparatively clean way from the shorter-range part, which needs to be approximated or parameterized

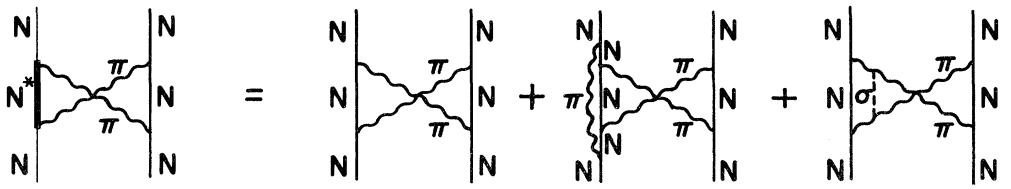

FIG. 7. Representative radiative corrections, whose sum can be represented by nucleon resonances (but only approximately in the narrow-width, or isobar, limit).

phenomenologically. The usual configuration-space description is a potential, local or nonlocal.

A potential description is of special utility if it can be used in a Schrödinger equation, for then the many-body problem can sometimes be treated with accuracy. M. Hossein Partovi and E. L. Lomon[8] have shown how the Blankenbecler-Sugar reduction of the Bethe-Salpeter amplitude could be extended to defining a potential which would generate the relativistic amplitude when used in the nonrelativistic Schrödinger equation. This method was applied in Ref. 8 to obtaining the nucleon-nucleon potential generated by the exchanges of single pions, η mesons, ρ mesons, and ω mesons and by the exchange of two pions. The result was qualitatively similar to realistic phenomenological potentials for ranges $r > \frac{1}{2}\mu^{-1}$.

In that calculation strong-interaction radiative corrections to single-meson exchange, such as those in Figs. 1(a), 1(c), and 1(d), were treated as renormalizations of coupling strengths or masses only. The momentum and energy dependences of these corrections were ignored because the vertex or propagator insertions were always of mass greater than that of the meson being exchanged. This large mass results in a slow dependence of the radiative correction on kinematical variables and is therefore absorbed into the renormalized constants with adequate accuracy.[9]

The decay of the ρ meson into two pions is an exception to the above type of radiative corrections, but was assumed to have a small effect on the q^2 dependence because of the relatively weak coupling (small width) of the ρ meson to two pions. The validity of that assumption will be discussed in Sec. V. Radiative corrections to two-meson exchange, as for example in Fig. 7, are related to nucleon-isobar intermediate states in πN scattering[1] which have not yet been treated in the program outlined by Ref. 8 for calculating the nucleon-nucleon potential from field theory.

The exchange of the σ meson was omitted in Ref. 8 because (a) the mass, the width, and even the existence of such a low-mass $T=0$, $J=0$ resonance were uncertain, and (b) if such a resonance did exist its width was certainly large enough to necessitate the calculation of diagrams such as Figs. 1(b) and 1(e). When the existence and nature of the σ meson (usually called the ϵ meson phenomenologically) became clearer[4,6,7] this calculation was undertaken by FPL.

They considered all the diagrams in Fig. 8. These are the diagrams in which the two nucleon lines can be separated by cutting a σ-meson line only, and so are called σ-exchange diagrams. Other diagrams containing σ mesons (see Figs. 2, 3, and 4 of FPL) are $\pi N\bar{N}$ vertex corrections [such as Fig. 1(a)] or are part of the $\pi N \to \pi N$ amplitude that must be considered together with nucleon isobar intermediate states, such as the last diagram of Fig. 7.

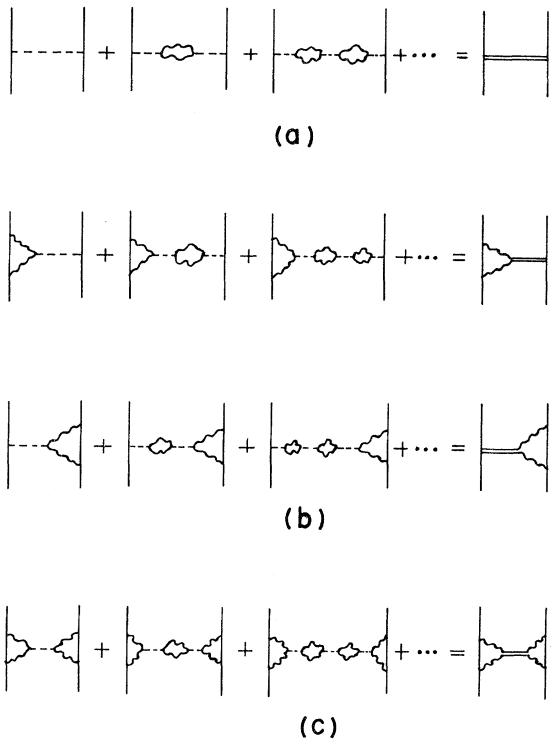

FIG. 8. Series of σ-exchange contributions to the nucleon-nucleon interaction, which are represented by a single "modified-propagator" σ-meson-exchange diagram. (a) ${}^{\Gamma}V^{\sigma}$, (b) ${}^{\Gamma}V^{\sigma\pi}$, (c) ${}^{\Gamma}V^{\sigma\pi\pi}$.

The leading diagram of each series (a), (b), and (c) of Fig. 8 (i.e., those without two-pion "bubble" insertions in the σ-meson propagator) was calculated accurately by FPL. In addition FPL approximated the effect of all orders of the pion-bubble insertions in Fig. 8(a) by averaging the potential given by a variable σ-meson mass, m, over a Breit-Wigner mass distribution:

$$V^{\Gamma}(r) = N^{-1} \int_{4\mu^2}^{\infty} V(r; m)\rho(M_\sigma, \Gamma_\sigma; m)\, dm^2, \qquad (23)$$

where $\rho(M_\sigma, \Gamma_\sigma; m) \equiv m^{-2}(m^2 - 4\mu^2)|\, G_{\mathrm{BW}}(q^2)|^2$ is the modulus of the Breit-Wigner amplitude [see Eq. (19)] for the σ resonance and $N = \int_{4\mu^2}^{\infty} \rho(M_\sigma, \Gamma_\sigma; m)\, dm^2$.

This approach (which we call the ρ-integral approach) is qualitatively, but not quantitatively, equivalent to the summation of pion-bubble diagrams (the modified-propagator approach). Equation (23) was not applied by FPL to Figs. 8(b) or 8(c) because the leading diagrams in those cases are already of approximately $\frac{1}{2}\mu^{-1}$ range owing to the two-pion vertices. The effect of Eq. (23) on spreading out the short-range potential of the first diagram of Fig. 8(a) is therefore more important. This is borne out by the present calculations; nevertheless, the spreading effect of the bubble insertions in Figs. 8(b) and 8(c) is not negligible.

The only parameters in the calculation of FPL are the physical mass and decay width of the σ meson, both of them now known within wide limits from analysis of high-energy pion-production experiments,[4,6,7] as discussed in Sec. II. It was also noted in Sec. II that the Weinberg[3] and Gell-Mann–Lévy[5] chiral models make predictions consistent with the experimental analysis. Both theoretical and experimental sources indicate that nucleon-nucleon potential predictions should be constrained by 500 MeV $\lesssim M_\sigma \lesssim$ 1200 MeV and 500 MeV $\lesssim \Gamma_\sigma \lesssim$ 1300 MeV.

Choosing values of M_σ and Γ_σ and using $(4\pi)^{-1} g_{\pi N}{}^2 = 14.4$, Eq. (14) [Eq. (12) of FPL], Eq. (22) [Eq. (1) of FPL], and Eq. (20) with $\bar{I}_B(M_\sigma{}^2)$ ignored [Eq. (3) of FPL] determined $g_{\sigma\pi}$ and $g_{\sigma N}$ in accordance with chiral conditions. The results (see Table I and Figs. 8–16 of FPL) showed the following.

(i) There is an important degree of cancellation between the leading diagrams of Figs. 8(a), 8(b), and 8(c).

(ii) The cancellation is better maintained over the medium-range values of r when the bubble diagrams of Fig. 8(a) are approximately taken into account by the ρ-integral method [Eq. (23)].

(iii) The resultant σ-exchange potential is Γ_σ dependent and is smallest at medium range for $\Gamma_\sigma \approx 620$ MeV.

(iv) For $\Gamma_\sigma \approx 620$ MeV the σ-exchange potential approximately cancels the "pair potential."[10]

(v) The addition of the σ-exchange potential for $M_\sigma \approx 765$ MeV and $\Gamma_\sigma \approx 620$ MeV improved the resemblance of the theoretical potential (which already had π, 2π, η, ρ, and ω exchange[8]) to the phenomenological Hamada-Johnston potential.[11]

The result (iii) shows that the chiral restrictions do not remove all ambiguity and that the effect may differ considerably from the extreme soft-pion assumption (no q dependence) made by Brown and Durso.[12] The more accurate calculations of this paper do not change any of the above results qualitatively but shift the values of Γ_σ for which cancellations occur. For $\Gamma_\sigma > 100$ MeV the σ-exchange potential predicted by the exact σ propagator differs in shape from that of the ρ-integral method.

We now use the modified σ-meson propagator to obtain an exact description of the potentials arising from Figs. 8(a), 8(b), and 8(c), including the bubble sum. The relativistic Feynman amplitude for the modified σ-propagator diagrams of those figures is reduced to a potential using the techniques of Ref. 8 and of FPL.[13] In momentum space we have ($\nabla^2 \equiv -q^2$; "c" stands for "central" and "so" stands for "spin orbit")

$$^{\Gamma}V_{\mathrm{c}}^{\sigma}(\Delta) = (2\pi)^{-3} g_{\sigma N}{}^2 \phi(\Delta^2) \bar{G}_\sigma(-\Delta^2), \qquad (24a)$$

$$^{\Gamma}V_{\mathrm{so}}^{\sigma}(\Delta) = -4(2\pi)^{-3} g_{\sigma N}{}^2 [\,\phi(\Delta^2) - 1]\, \bar{G}_\sigma(-\Delta^2), \qquad (24b)$$

$$^{\Gamma}V_{\mathrm{c}}^{\sigma\pi}(\Delta) = -3(2\pi)^{-5} g_{\sigma\pi} g_{\sigma N} g_{\pi N}{}^2 M \times \phi(\Delta^2) \bar{G}_\sigma(-\Delta^2) R(-\Delta^2), \qquad (24c)$$

$$^{\Gamma}V_{\mathrm{so}}^{\sigma\pi}(\Delta) = 12(2\pi)^{-5} g_{\sigma\pi} g_{\sigma N} g_{\pi N}{}^2 M \times [\,\phi(\Delta^2) - 1]\, \bar{G}_\sigma(-\Delta^2) R(-\Delta^2), \qquad (24d)$$

$$^{\Gamma}V_{\mathrm{c}}^{\sigma\pi\pi}(\Delta) = -9(\tfrac{1}{2})^3 (2\pi)^{-7} g_{\sigma\pi}{}^2 g_{\pi N}{}^4 M^2 \times \phi(\Delta^2) \bar{G}_\sigma(-\Delta^2) [\,R(-\Delta^2)]^2, \qquad (24e)$$

$$^{\Gamma}V_{\mathrm{so}}^{\sigma\pi\pi}(\Delta) = 9(\tfrac{1}{2})(2\pi)^{-7} g_{\sigma\pi}{}^2 g_{\pi N}{}^4 M^2 \times [\,\phi(\Delta^2) - 1]\, \bar{G}_\sigma(-\Delta^2) [\,R(-\Delta^2)]^2, \qquad (24f)$$

where

$$\phi(\Delta^2) = [\,1 + (2M)^{-2}\Delta^2\,]^{1/2} \qquad (25)$$

and [as defined by Eq. (37) of FPL]

$$R(-\Delta^2) = \int_0^1 y(1-y)^{-1} dy \times \int_0^1 x(1-x)^{-1} [\,\Delta^2 + \tau_{xy}\,]^{-1} dx \qquad (26)$$

with

$$\tau_{xy}=x^{-1}(1-x)^{-1}(1-y)^{-1}[M^2x^2y^2+\mu^2(1-xy)]. \tag{27}$$

The configuration-space potentials are obtained here by numerically evaluating the Fourier transform directly from

$$V_c(r)=4\pi r^{-1}\int_0^\infty \Delta\sin\Delta r V_c(\Delta)\,d\Delta \tag{28}$$

and

$$V_{so}(r)=-4\pi r^{-3}\int_0^\infty \Delta^{-1}(\sin\Delta r-\Delta r\cos\Delta r)\times V_{so}(\Delta)\,d\Delta, \tag{29}$$

with $V_c(\Delta)$ [$V_{so}(\Delta)$] obtained from Eqs. (24a), (24c), or (24e) [Eqs. (24b), (24d), or (24f)] to generate ${}^\Gamma V_c^\sigma(r)$, ${}^\Gamma V_c^{\sigma\pi}(r)$, or ${}^\Gamma V_c^{\sigma\pi\pi}(r)$ [${}^\Gamma V_{so}^\sigma(r)$, ${}^\Gamma V_{so}^{\sigma\pi}(r)$, or ${}^\Gamma V_{so}^{\sigma\pi\pi}(r)$], respectively.

In the present work it was not found to be convenient to use the pole approximations to Eqs. (28) and (29) which were used in FPL. In FPL the pole approximation was shown to lead to negligible error ($<1\%$), which has been confirmed by the present method of calculation. However, the use of the pole approximation to Eq. (26) for $R(-\Delta^2)$ resulted in the need for numerical integration over both the variables x and y instead of the analytic integration over x [Eq. (37) of FPL] which we can use for $R(-\Delta^2)$ in Eqs. (24). Consequently there is a computing advantage as well as greater accuracy in the direct use of Eqs. (28) and (29) as regards ${}^\Gamma V^{\sigma\pi}$ and ${}^\Gamma V^{\sigma\pi\pi}$. Moreover, the present modified-propagator method does not require another integration in order to obtain the spreading due to the σ-meson width as does the ρ-integral method [Eq. (23)]. It follows that even ${}^\Gamma V^\sigma$ is no harder to compute without the pole approximation than was $V^{\Gamma\sigma}$ of FPL with the pole approximation.

Analogously to FPL we define the total central and spin-orbit σ-exchange contributions to the potential:

$${}^\Gamma V_c^{\sigma E}(r)\equiv {}^\Gamma V_c^\sigma(r)+{}^\Gamma V_c^{\sigma\pi}(r)+{}^\Gamma V_c^{\sigma\pi\pi}(r) \tag{30}$$

and

$${}^\Gamma V_{so}^{\sigma E}(r)\equiv {}^\Gamma V_{so}^\sigma(r)+{}^\Gamma V_{so}^{\sigma\pi}(r)+{}^\Gamma V_{so}^{\sigma\pi\pi}(r). \tag{31}$$

We note that there are no spin-spin or tensor contributions of σ exchange; hence $V_{ss}^{\sigma E}=V_T^{\sigma E}=0$.

IV. RESULTS FOR THE σ-EXCHANGE CONTRIBUTION TO THE NUCLEON-NUCLEON FORCE

The strong decay of the σ meson into two pions affects the σ-exchange contribution to the nucleon-nucleon force through (i) the renormalization of the $\sigma N\bar{N}$ vertex, (ii) the momentum dependence of the vertex corrections represented by $V^{\sigma\pi}$ and $V^{\sigma\pi\pi}$ [the leading diagram of Fig. 8(b) and of Fig. 8(c)], and (iii) the modification of the σ-meson propagator via the "bubble sums" in Fig. 8. The effect (ii) was completely and accurately treated in FPL. That reference also treated effect (i) in the approximation that the modification of the propagator, represented by the term $\mathrm{Re}\bar{I}_B(M_\sigma^2)$ considered in Eq. (20), was ignored. FPL also treated effect (iii) but treated it only for V^σ and then only in the ρ-integral approximation. The full and accurate treatment of (iii) and the propagator-related modification of (i) is the contribution of the present paper.

To investigate the effect of the total σ-meson exchange and especially that of the propagator modification we have made calculations for M_σ of 500 and 765 MeV and for Γ_σ of 100, 300, 620, 1193, and 2386 MeV. $\Gamma_\sigma^{\mathrm{crit}}=625.2$ MeV for $M_\sigma=765$ MeV [see Eq. (15) and Fig. 4], and $\Gamma_\sigma^{\mathrm{crit}}=458$ MeV

TABLE I. σ-meson coupling constants determined by Γ_σ and the chiral condition with $g_{\pi N}^2/4\pi=14.4$. [$g_{\sigma N}^*$ is obtained from Eq. (20) by setting $\mathrm{Re}\bar{I}_B(M_\sigma^2)=0$. This corresponds to ignoring the modification of the σ-meson propagator, as in FPL.]

Γ_σ (MeV)	M_σ (MeV)	$g_{\sigma\pi}^2/4\pi\mu^2$ [Eq. (14)]	$(g_{\sigma N}^R)^2/4\pi$ [Eq. (22)]	$g_{\sigma N}^2/4\pi$ [Eq. (20)]	$(g_{\sigma N}^*)^2/4\pi$
100	765	2.81	343.59	387.0	423.8
	500	2.06	77.77	112.3	111.8
300	765	8.43	114.53	160.6	203.1
	500	6.19	25.92	66.7	66.1
620	765	17.43	55.42	105.6	157.5
	500	12.78	12.54	63.4	62.6
1193	765	33.53	28.80	86.4	154.9
	500	24.60	6.52	75.5	74.3
2386	765	67.07	14.40	87.4	190.7
	500	49.20	3.26	109.9	107.8

for $M_\sigma = 500$ MeV. When considering the cases with $\Gamma_\sigma > \Gamma_\sigma^{\text{crit}}$ for nucleon-nucleon scattering one must take into account the need to shift or eliminate the pole in pion-pion scattering. Table I gives the values of $g_{\sigma\pi}$, $g_{\sigma N}$, and $g_{\sigma N}^R$ for the chosen values of M_σ and Γ_σ. As stated previously, the Weinberg model[3] corresponds to $M_\sigma = 765$ MeV and, if $g_A/g_V = 1.37$, to $\Gamma_\sigma = 620$ MeV or, if $g_A/g_V = 1$, to $\Gamma_\sigma = 1193$ MeV. The Gell-Mann–Lévy model[5] corresponds to any mass and, if $g_A/g_V = 1.37$, to $\Gamma_\sigma = 1193$ MeV, or, if $g_A/g_V = 1$, to $\Gamma_\sigma = 2386$ MeV. Masses between 500 and 1200 MeV and widths between 500 and 1300 MeV seem consistent with high-energy production experiments.[4,6,7] The smaller widths (100 and 300 MeV) are used to examine the behavior as the width decreases.

In Fig. 9 we illustrate the effect on the range dependence of each type of diagram [Fig. 8(a), 8(b), or 8(c)] of the propagator modification. The figure gives the ratios of $V^\sigma(r)$, $V^{\sigma\pi}(r)$, or $V^{\sigma\pi\pi}(r)$ to ${}^\Gamma V^\sigma(r)$, ${}^\Gamma V^{\sigma\pi}(r)$, or ${}^\Gamma V^{\sigma\pi\pi}(r)$, respectively, for both central and spin-orbit cases. The first three represent the leading diagram of Fig. 8(a), 8(b), or 8(c) and are obtained by replacing $\bar{G}_\sigma$ in Eqs. (24) by $(q^2 - M_\sigma^2)^{-1}$ and also dropping $\bar{I}_B$ terms in Eq. (20), while still using Eq. (14) to relate $g_{\sigma\pi}$ to Γ_σ.

The numerators $V^\sigma(r)$, $V^{\sigma\pi}(r)$, or $V^{\sigma\pi\pi}(r)$ are therefore just as defined in FPL, with negligible numerical differences due to the pole approximation used in FPL. The denominators are defined in this paper and represent the extra ef-

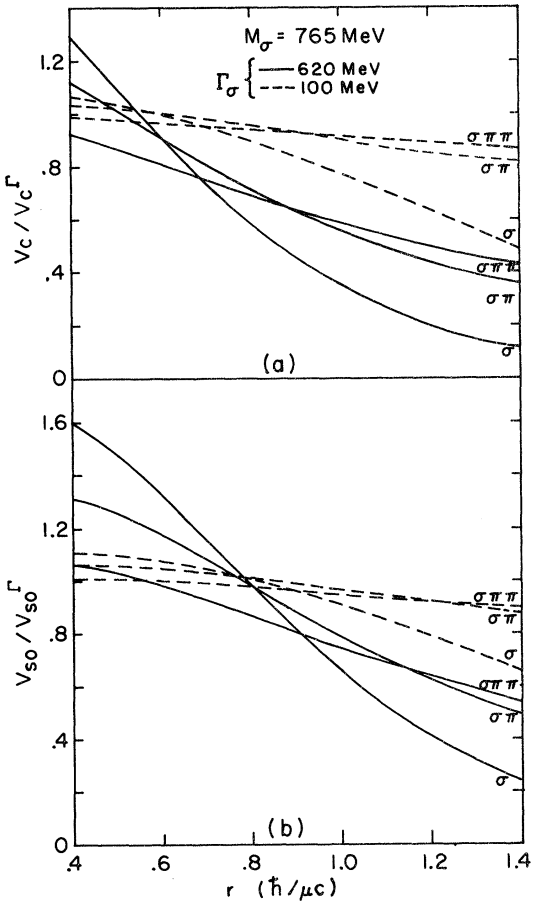

FIG. 9. Effect of pion-bubble sums. Ratios of potentials obtained with unmodified σ-meson propagators to potentials obtained with σ-meson propagators modified by the pion-bubble sum. The ratios are shown for (a) the central potential and (b) the spin-orbit potential contributed by the chiral σ exchange (σ), the σ exchange decaying to two pions absorbed on one nucleon ($\sigma\pi$), and the σ exchange decaying to two pions at each end absorbed on each nucleon ($\sigma\pi\pi$). The solid lines are for $\Gamma_\sigma = 620$ MeV and the dashed lines for $\Gamma_\sigma = 100$ MeV. $M_\sigma = 765$ MeV.

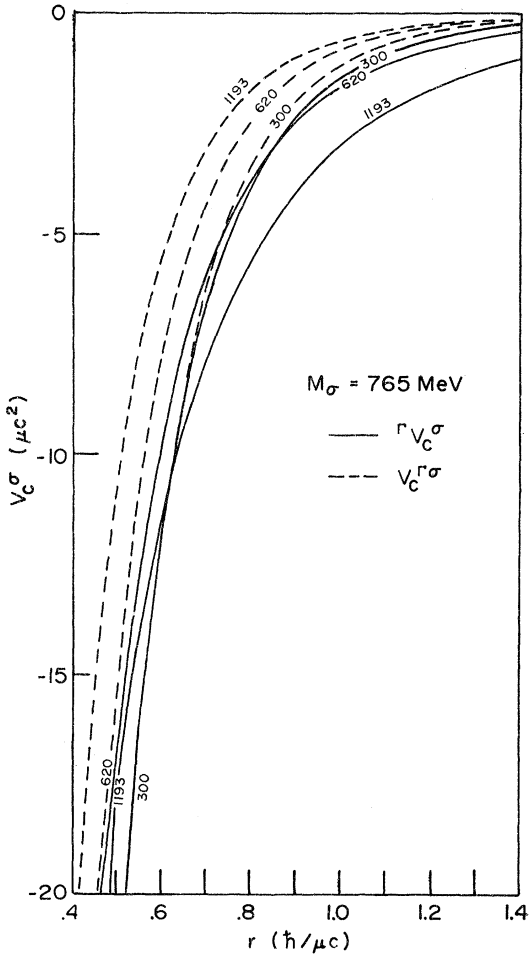

FIG. 10. Comparison of the bubble-sum method and the mass-distribution approximation: central potential. The direct σ-exchange central potential is plotted for different values of Γ_σ (indicated in the curves in MeV) as given by the pion-bubble-sum method (solid lines) and by the method of integrating over a Breit-Wigner mass distribution (dashed lines). $M_\sigma = 765$ MeV.

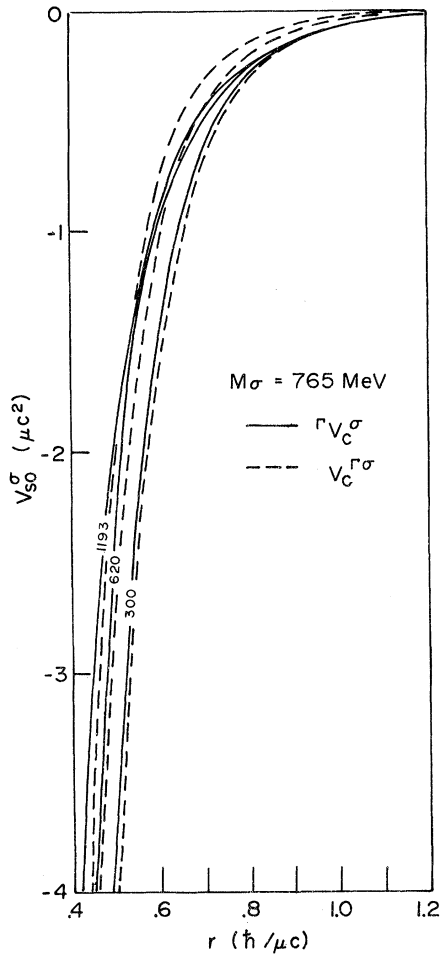

FIG. 11. Comparison of the bubble-sum method and the mass-distribution approximation: spin-orbit potential. Same as figure 10 for the direct σ-exchange spin-orbit potential.

fect of the propagator modification. As expected, the ratio decreases with r owing to the spreading to larger r caused by the width of the σ meson. Moreover, the decrease with r is most rapid for $V^{\sigma}(r)$, next for $V^{\sigma\pi}(r)$, and least for $V^{\sigma\pi\pi}(r)$, as expected from the range of the leading diagrams without pion "bubbles." Finally, the size of the effect is controlled by Γ_σ, being relatively smaller for $\Gamma_\sigma = 100$ MeV than for $\Gamma_\sigma = 620$ MeV. The ratios are similar for the central and spin-orbit parts [Figs. 9(a) and 9(b), respectively]. For none of the cases illustrated is the effect negligible, except perhaps for $V^{\sigma\pi\pi}(r)$ with $\Gamma_\sigma = 100$ MeV.

Figures 10 and 11 compare the approximate spreading of $V^{\sigma}(r)$ obtained by the ρ-integral method, $V^{\Gamma\sigma}(r)$ of FPL, with the result of the exact propagator modification, $^{\Gamma}V^{\sigma}(r)$, for central (Fig. 10) and spin-orbit cases (Fig. 11). It is seen that

TABLE II. The values of the central σ-meson exchange potential contributions of Eqs. (24)–(29) and Figs. 8(a), 8(b), and 8(c). $M_\sigma = 765$ MeV, $\Gamma_\sigma = 620$ MeV.

r ($\hbar/\mu c$)	$^{\Gamma}V_c^{\sigma}$ (μc^2)	$^{\Gamma}V_c^{\sigma\pi}$ (μc^2)	$^{\Gamma}V_c^{\sigma\pi\pi}$ (μc^2)	$^{\Gamma}V_c^{\sigma E}$ (μc^2)
0.4	−31.14	30.89	−6.68	−6.93
0.5	−16.90	18.38	−4.34	−2.86
0.6	− 9.83	11.45	−2.89	−1.27
0.7	− 6.02	7.39	−1.97	−0.596
0.8	− 3.83	4.90	−1.37	−0.293
0.9	− 2.52	3.33	−0.96	−0.150
1.0	− 1.69	2.30	−0.68	−0.080
1.1	− 1.16	1.61	−0.49	−0.045
1.2	− 0.81	1.15	−0.36	−0.026
1.3	− 0.58	0.82	−0.26	−0.016
1.4	− 0.41	0.60	−0.193	−0.010

for $\Gamma_\sigma = 300$ MeV the effects are very much the same [while differing considerably from the no-spreading case $V^{\sigma}(r)$ as implied by Fig. 9]. For $\Gamma_\sigma = 620$ MeV there is significant difference in shape; the exact method causes more spreading, but little difference in normalization. By $\Gamma_\sigma = 1193$ MeV the exact calculation differs considerably from the ρ-integral calculation not only in shape (much more spread to large range) but also in normalization, causing the $\Gamma_\sigma = 1193$ MeV case to be more attractive at medium range than the $\Gamma_\sigma = 620$ MeV case, as well as at long range.

Tables II and III give the values of $^{\Gamma}V^{\sigma E}$ and its parts for the central and spin-orbit potentials, respectively (see Fig. 12) with $M_\sigma = 765$ MeV and $\Gamma_\sigma = 620$ MeV. The large amount of cancellation among $^{\Gamma}V^{\sigma}$, $^{\Gamma}V^{\sigma\pi}$, and $^{\Gamma}V^{\sigma\pi\pi}$ is evident. The total σ-exchange potential contributions are shown in Figs. 13–16 for several values of Γ_σ and M_σ and are also compared with $V_c^{\rm pair}$ and $V_{so}^{\rm pair}$ (the potentials arising in the static limit of time-ordered graphs with one- and two-nucleon-pair intermediate states[10]). The Weinberg model[3] (M_σ

TABLE III. The values of the spin-orbit σ-meson exchange potential contributions of Eqs. (24)–(29) and Figs. 8(a), 8(b), and 8(c). $M_\sigma = 765$ MeV, $\Gamma_\sigma = 620$ MeV.

r ($\hbar/\mu c$)	$^{\Gamma}V_{so}^{\sigma}$ (μc^2)	$^{\Gamma}V_{so}^{\sigma\pi}$ (μc^2)	$^{\Gamma}V_{so}^{\sigma\pi\pi}$ (μc^2)	$^{\Gamma}V_{so}^{\sigma E}$ (μc^2)
0.4	−6.28	4.73	−0.79	−2.35
0.5	−2.36	2.07	−0.39	−0.69
0.6	−1.01	0.99	−0.21	−0.23
0.7	−0.48	0.51	−0.12	−0.085
0.8	−0.25	0.28	−0.07	−0.034
0.9	−0.13	0.16	−0.04	−0.014
1.0	−0.076	0.095	−0.026	−0.006
1.1	−0.045	0.058	−0.016	−0.003
1.2	−0.027	0.037	−0.011	−0.001
1.3	−0.017	0.023	−0.007	−0.0007
1.4	−0.011	0.015	−0.005	−0.0003

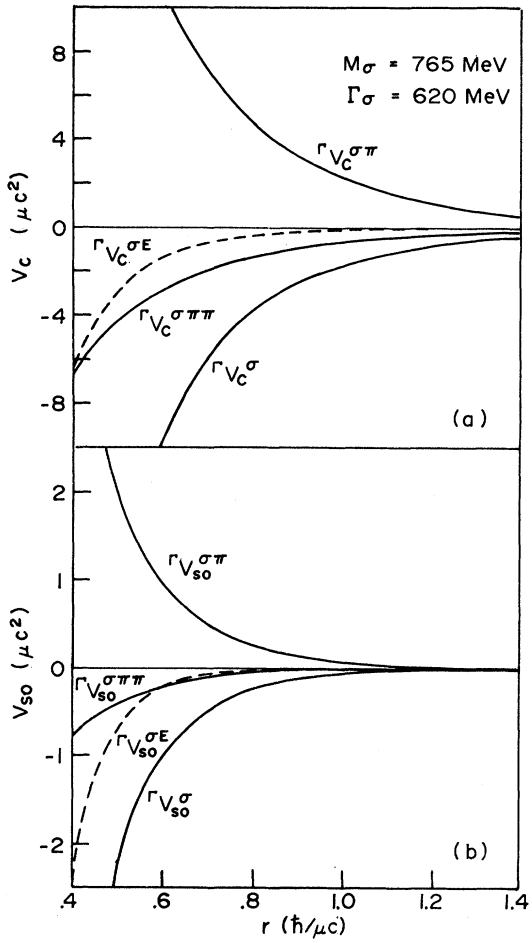

FIG. 12. The parts of the σ-exchange potential ${}^{\Gamma}V^{\sigma}$, ${}^{\Gamma}V^{\sigma\pi}$, ${}^{\Gamma}V^{\sigma\pi\pi}$ are compared with the sum ${}^{\Gamma}V^{\sigma E}$, for the (a) central and (b) spin-orbit potentials. The case corresponds to $M_\sigma = 765$ MeV and $\Gamma_\sigma = 620$ MeV. (See Tables II and III.) The varying signs of the parts lead to a large degree of cancellation, which is nearly complete for $\Gamma_\sigma = 1193$ MeV.

$= 765$ MeV and $\Gamma_\sigma = 620$ MeV correspond to $g_V/g_A = 1.37$) very nearly cancels the "pair" potentials, even more so than in FPL (see Figs. 8 and 9 of FPL).

Thus, as suggested by Weinberg, the good asymptotic behavior of the model tends to extend the range of q which chiral conditions are maintained. For other values of Γ_σ, although the chiral condition is imposed so that the diagrams in Fig. 6 cancel the diagram of Fig. 2(a), the "pair" potential is not fully canceled at most ranges because of the q dependence of the diagrams. This effect can be called "hard-pion" corrections. What our specific Lagrangian illustrates is that the hard-pion correction can be large at moderate values of momentum transfer, especially when $\Gamma_\sigma \lesssim 300$ MeV. The "softness"

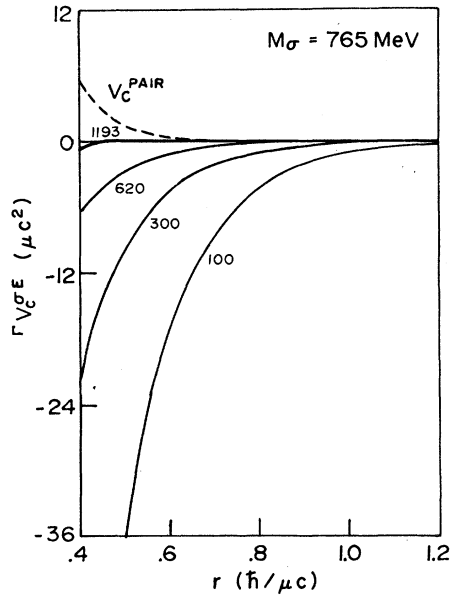

FIG. 13. The total σ-exchange central potentials and the nonrelativistic "pair potential." The σ-exchange central potentials ${}^{\Gamma}V_c^{\sigma E} = {}^{\Gamma}V_c^{\sigma} + {}^{\Gamma}V_c^{\sigma\pi} + {}^{\Gamma}V_c^{\sigma\pi\pi}$ using the bubble-sum method are given for the values of Γ_σ indicated on the curves in MeV and with $M_\sigma = 765$ MeV. The V_c^{pair} is the adiabatic limit of the sum of time-ordered two-pion-exchange diagrams with one and two nucleon pairs.

of the Lagrangian is also dependent on the σ-meson mass. For $M_\sigma = 500$ MeV and $\Gamma_\sigma = 620$ MeV Fig. 14 shows that ${}^{\Gamma}V_{so}^{\sigma E}$ only cancels about half of V_{so}^{pair} although ${}^{\Gamma}V_c^{\sigma E}$ still cancels V_c^{pair} quite well at medium range.

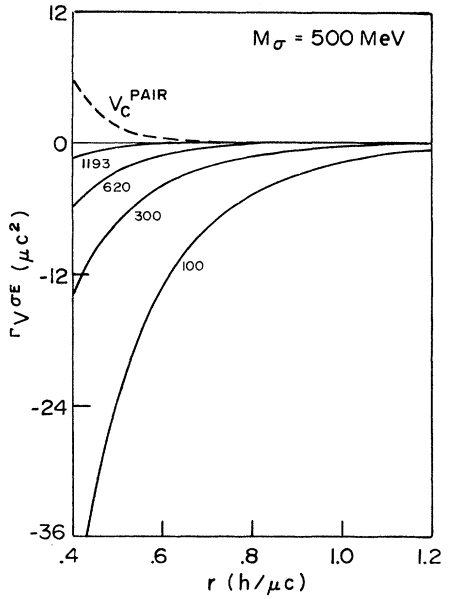

FIG. 14. The total σ-exchange central potentials and the nonrelativistic "pair potential." Same as Fig. 13 for $M_\sigma = 500$ MeV.

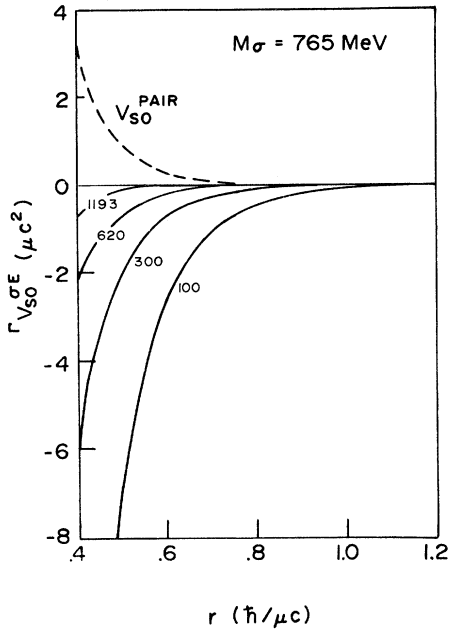

FIG. 15. The total σ-exchange spin-orbit potentials and the nonrelativistic "pair potential." Same as Fig. 13 for the spin-orbit potentials and $M_\sigma = 765$ MeV.

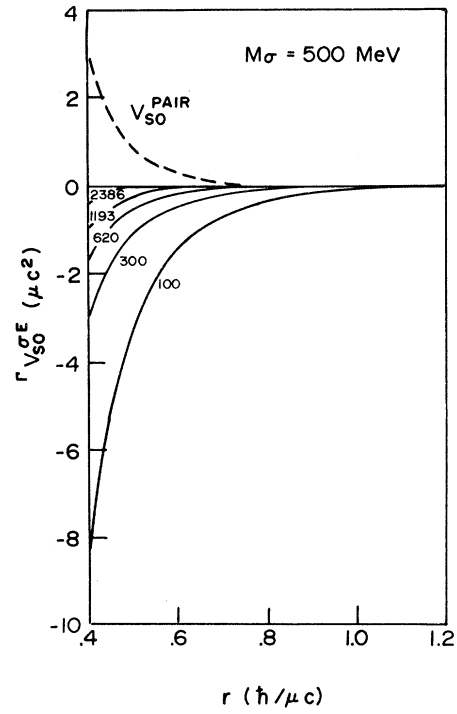

FIG. 16. The total σ-exchange spin-orbit potentials and the nonrelativistic "pair potential." Same as Fig. 15 for $M_\sigma = 500$ MeV.

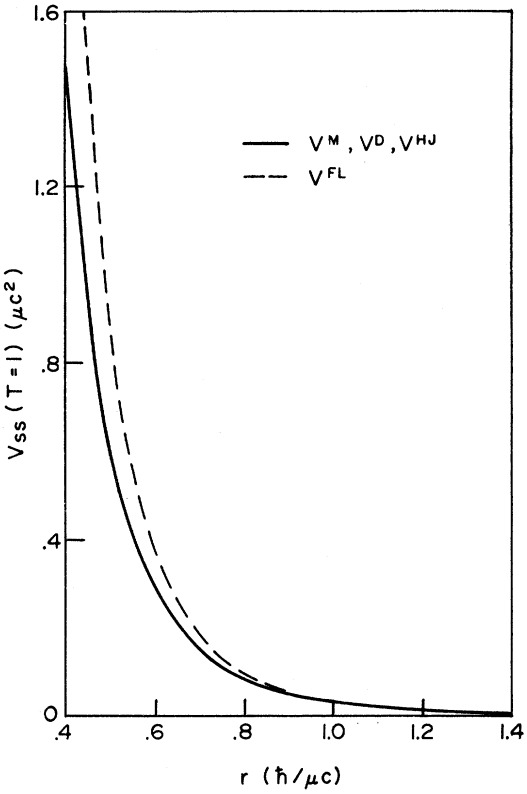

FIG. 17. Comparison of various nucleon-nucleon $T = 1$ spin-spin potentials. The meson-theoretical potential V^M of Ref. 8 is compared with the dispersion-theoretical potential V^D of Ref. 16, the adiabatic meson-theoretical potential V^{FL} of Ref. 15, and the phenomenological Hamada-Johnston potential V^{HJ} of Ref. 11. As σ exchange does not contribute to the spin-spin or tensor potentials, V^M represents the one- and two-pion and one-boson exchange potential.

Figures 13 and 15 show that ${}^\Gamma V_c^{\sigma E}$ and ${}^\Gamma V_{so}^{\sigma E}$ both nearly vanish for $r \gtrsim 0.4\mu^{-1}$ when $M_\sigma = 765$ MeV and $\Gamma_\sigma = 1193$ MeV. In spite of the large value of $g_{\sigma N}^R$ the resulting potential is negligible because of the cancellation occurring between the three classes of diagrams, Figs. 8(a), 8(b), and 8(c). The use of the contribution of Fig. 8(a) alone, with values of $g_{\sigma N}^R$ of the order indicated by theories such as Refs. 3 and 5, leads to much larger σ-meson-exchange predictions. Consequently, one-boson-exchange fits[14] have σ-meson (or ϵ-meson) coupling constants (squared) about $\frac{1}{4}$ that of theoretical models.[3,5]

Figures 17–24 illustrate the total theoretical potential obtained by adding ${}^\Gamma V^{\sigma E}$ for $M_\sigma = 765$ MeV and $\Gamma_\sigma = 620$ MeV to the potential, V^M, previously calculated for exchange of π, 2π, η, ρ, and ω mesons.[8] For comparison those figures also include the medium- and long-range parts

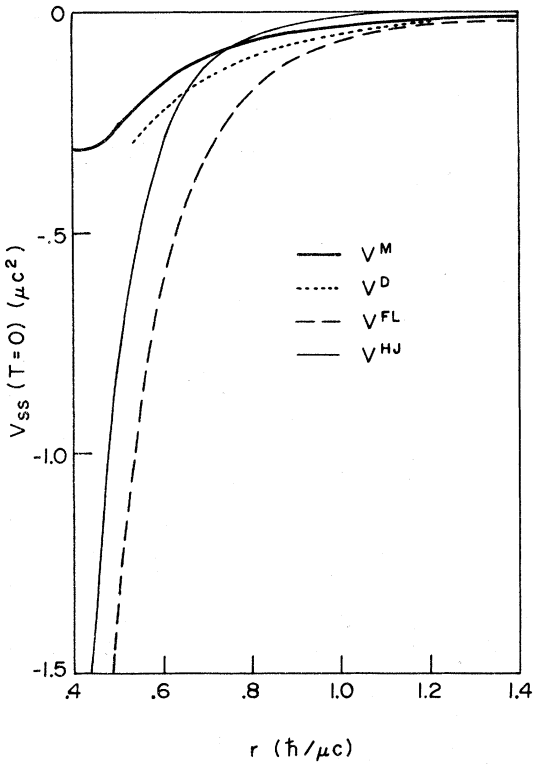

FIG. 18. Comparison of various nucleon-nucleon $T=0$ spin-spin potentials. Same potentials as Fig. 17.

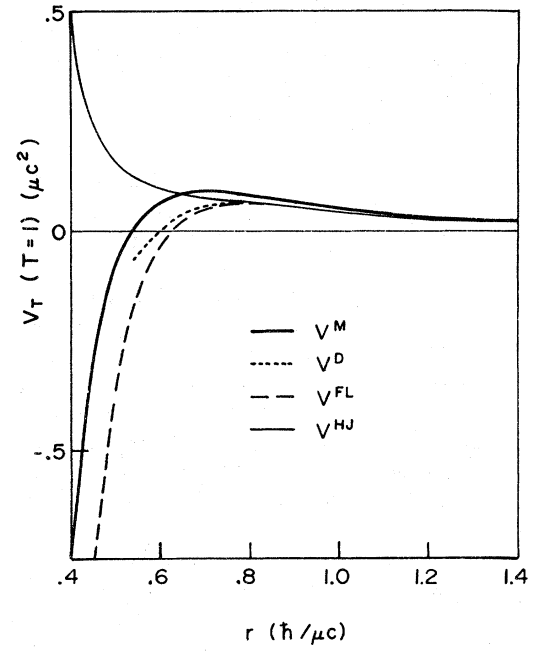

FIG. 19. Comparison of various nucleon-nucleon $T=1$ tensor potentials. Same potentials as Fig. 17.

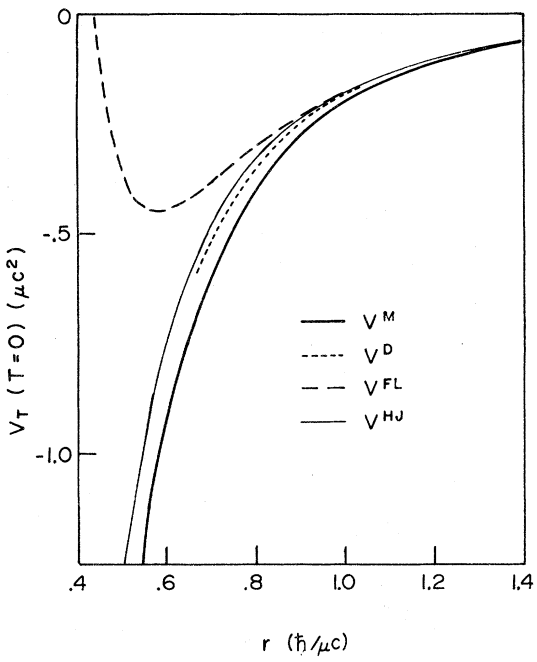

FIG. 20. Comparison of various nucleon-nucleon $T=0$ tensor potentials in the $^3S_1$ state. Same potentials as Fig. 17.

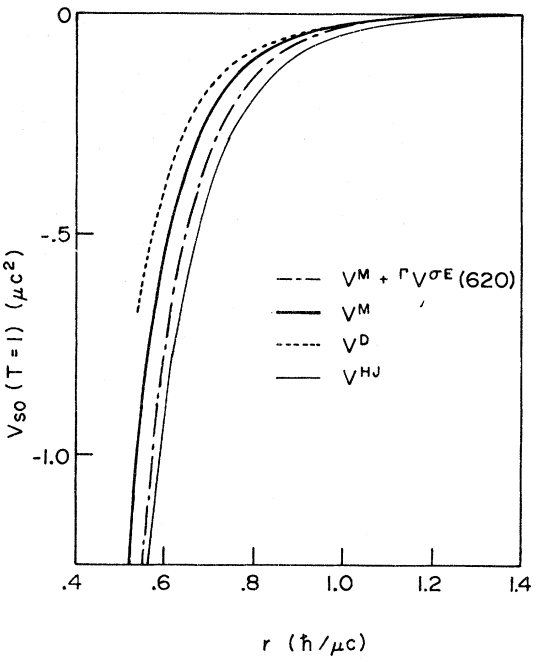

FIG. 21. Comparison of various nucleon-nucleon $T=1$ spin-orbit potentials. In addition to the potentials described in Fig. 17 the effect of adding ${}^{\Gamma}V^{\sigma E}$ is shown for $M_\sigma = 765$ MeV and $\Gamma_\sigma = 620$ MeV. As ${}^{\Gamma}V^{\sigma E}(1193)$ is very small, V^M also represents a σ-meson exchange of that width. $V_{SO}^{FL} = 0$ for $T=1$ and $T=0$.

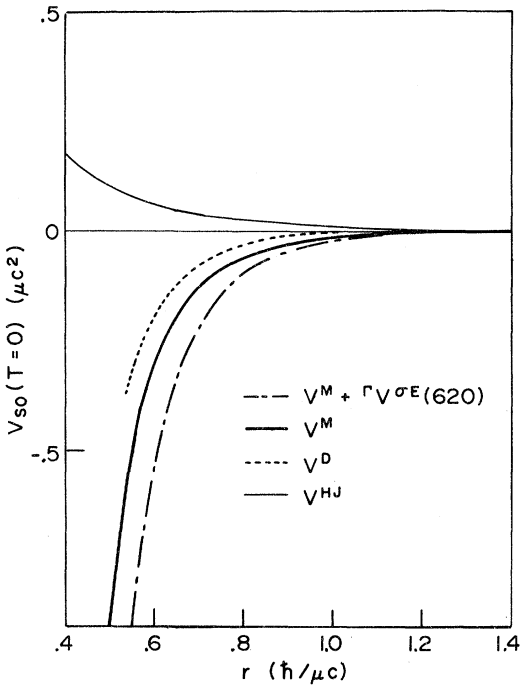

FIG. 22. Comparison of various nucleon-nucleon $T=0$ spin-orbit potentials. Same potentials as Fig. 21.

of V^M itself and of three realistic potentials, that of Hamada and Johnston,[11] V^{HJ}, that of Feshbach and Lomon,[15] V^{FL}, and that of Lacombe *et al.*[16], V^D. All of these potentials fit the nucleon-nucleon-scattering and deuteron data moderately well and all have one-pion-exchange long-range tails. The

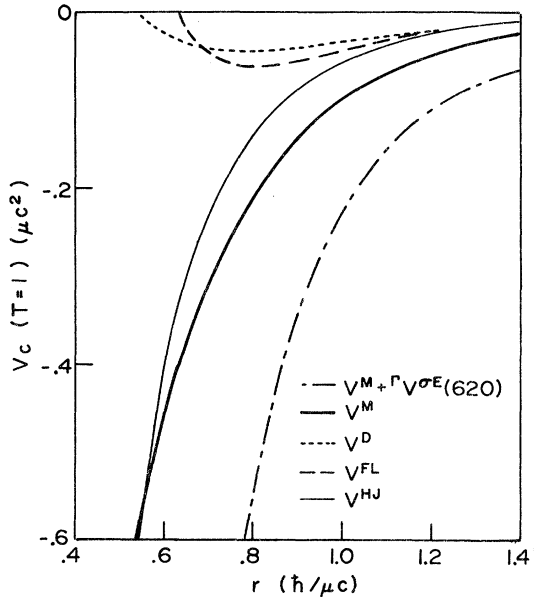

FIG. 23. Comparison of various nucleon-nucleon $T=1$ central potentials. Same potentials as Fig. 21.

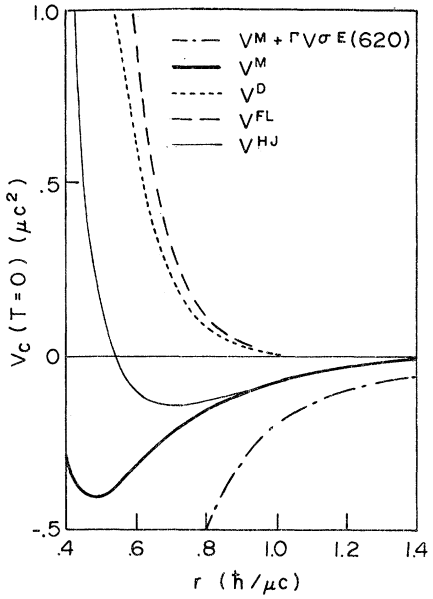

FIG. 24. Comparison of various nucleon-nucleon $T=0$ central potentials. Same potentials as Fig. 21.

medium-range part of the potential of Ref. 11 is phenomenological, as are the short-range parts of all three. The medium-range potential of Ref. 15 is theoretical, including the same exchanges as in Ref. 8, but in the static limit. Reference 16 is a recent dispersion-theoretical calculation of the medium-range potential, but includes a phenomenological core contribution for $r \lesssim 0.7\mu^{-1}$.

Figures 17–20 show that in both the $T=1$ and $T=0$ states the spin-spin and tensor-meson theoretical potentials of Ref. 8, V^M, are quantitatively similar to the dispersion-theoretical potentials of Ref. 16, V^D. As $V^{\sigma E}$ vanishes in these states, the similarity of V^M and V^D indicates that the intermediate isobar contributions neglected in V^M may be small in the tensor and spin-spin potentials. Moreover, as it was recently shown that the V^D potential is phenomenologically consistent with a boundary-condition core,[17] it can be inferred that V^M will also be able to fit the tensor and spin-spin components with a boundary-condition core.

For both the $T=1$ and $T=0$ spin-orbit potentials, Figs. 21 and 22, we notice that V^M is again similar to V^D, although slightly more attractive. However, $V^M + V^{\sigma E}(620)$ is substantially more attractive than V^D in both cases. This difference is not very significant phenomenologically: Because of the short range nature of the spin-orbit potentials the data can be fitted by varying the core properties. That can be inferred by noticing that both V^D and V^{FL} can fit the data with a bound-

ary-condition core[15,17] even though the latter has *no* medium-range spin-orbit potential. A shift in value of the boundary condition makes up for the difference.

In the central potentials, Figs. 23 and 24, the differences are more serious (because of the phenomenological core in V^D one need only compare for $r \gtrsim 0.7\mu^{-1}$). In both the $T=1$ and $T=0$ cases V^M is much more attractive than V^D, and it is also substantially more attractive than V^{HJ} for $T=1$. In these cases ${}^{\Gamma}V^{\sigma E}(620)$ is attractive and significantly increases the above disparities. As intermediate-isobar corrections to V^M are attractive, they would only make the disparity worse if added to V^M. About half of the difference between V^M and V^D is due to the choice of $\omega N\bar{N}$ coupling constant. The ω-exchange contribution is repulsive and large in the central potentials, especially in V^D, for which $g_{\omega N}{}^2/4\pi = 9.52$. In V^M the value is $g_{\omega N}{}^2/4\pi = 6.36$. The rest of the discrepancy between V^M and V^D (in both the constant and spin-orbit potentials) is likely to be due to the different treatments of two-pion exchange with pion-pion interaction.

In V^M the two-pion noninteracting continuum is supplemented by the decaying σ-meson exchange as derived in this article. The σ-exchange contribution is attractive for $\Gamma_\sigma = 620$ MeV, only becoming repulsive for $\Gamma_\sigma \gtrsim 1193$ MeV. By contrast the noninteracting two-pion continuum in V^D is supplemented by the difference between the total two-pion-amplitude contribution and the $T=0$, $J=0$ projection of the continuum. This supplement is in the right direction to account for the disparity between V^D and V^M, as the above difference is positive.

The present article does not consider any pion-pion interaction other than through the σ meson. The small experimental pion-pion scattering length is an indication that there is a repulsive interaction in the background (resonance fits give a larger scattering length[4,6,7]). Diagrams that provide such background pion-pion repulsion could in principle be added to the meson theoretical descriptions of the nucleon-nucleon potential.

When $\Gamma_\sigma = 1193$ MeV and $M_\sigma = 765$ MeV the values of $V_c^{\sigma E}$ and $V_{so}^{\sigma E}$ are negligible at medium and long range. Hence the need for additional pion-pion interaction contributions is less if we choose such values of Γ_σ. Nevertheless, the $T=1$ central meson theoretical potential is still likely to need a substantial correction.

In addition it must be remembered that $\Gamma_\sigma = 1193$ MeV entails a pole in the modified propagator, which in turn implies a pion-pion state in the absence of strong exchange effects. As $\Gamma_\sigma^{\text{crit}}$ depends on M_σ, the situation may be improved by choosing a value of M_σ for which $\Gamma_\sigma^{\text{crit}}$ is larger than 625 MeV.

V. OTHER APPLICATIONS FOR THE MODIFIED PROPAGATOR

It was remarked in Sec. III that the ρ-meson decay into two pions presents similar complications for ρ exchange as for the σ-meson case, but the effect was expected to be less severe because of the smaller ρ-meson width. Because of differences in spin and isospin the σ-meson equations of this paper cannot be directly applied to the ρ-meson case. However, a qualitative indication of the severity of the complications for the ρ exchange may be obtainable by using the appropriate ρ-decay width and $\rho N\bar{N}$ coupling strength in the σ-meson equations.

There is no equivalent constraint to Eq. (22) for the ρ meson. To simulate ρ exchange qualitatively a value of $g_{\sigma\pi}$ was used as determined from Eq. (14) with $\Gamma_\sigma = 100$ MeV and $M_\sigma = 765$ MeV the width and mass of the ρ meson. The criterion for $g_{\sigma N}$ [with $g_{\sigma N}^R$ determined by Eq. (20)] was that the resulting central potential be of similar strength to the central simple ρ-exchange potential (see Fig. 11 of Ref. 8).

We must take the ρ-meson spin into account when renormalizing the $\rho N\bar{N}$ coupling constant with diagrams analogous to Fig. 6. The term proportional to $R(0)$ in Eq. (20) will vanish as it will have a q^2 factor due to the p state of the two pions, and Fig. 6 is evaluated at $q^2 = 0$. The correction term $M_\sigma{}^{-2}\mathrm{Re}\bar{I}_\beta(M_\sigma{}^2)$ will remain, as it corresponds to the mass renormalization, but this is only 0.05 for $g_{\sigma\pi} = +5.94$ as determined by the ρ-meson width. Hence $g_{\sigma N}^R \approx g_{\sigma N} \approx \pm 4$ in order to obtain a simple scalar-exchange potential of the same magnitude as the simple ρ-exchange central potentials. With $g_{\sigma\pi} \approx g_{\sigma N} \approx 5$ the contributions of Figs. 8(b) and 8(c) are of the same order as that of Fig. 8(a). Of course, spin and isospin effects will modify all three diagrams and may

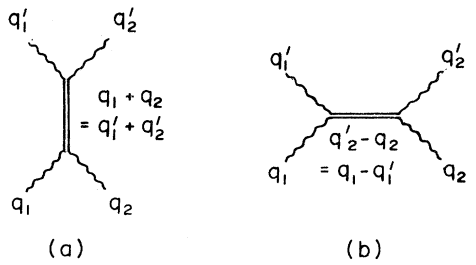

FIG. 25. σ-meson contributions to pion-pion scattering. (a) A σ-meson contribution containing all pion-"bubble" contributions in the intermediate state. (b) A σ-meson exchange containing all pion-"bubble" contributions.

well enhance the ratio of Fig. 8(a) to the others, but a full calculation along the lines of the present σ-meson calculation is needed in order to determine whether the corrections to simple ρ exchange are important.

Pion-pion scattering, insofar as it is mediated by σ-meson exchange, has contributions from both Fig. 25(a) and Fig. 25(b), each of which includes the "bubble sum." The first diagram contributes only to the $I=0$ pion-pion state, but the second diagram contributes to all three isospin states. The q^2 dependence of Fig. 25(b) is given by Eq. (11), while the contribution of Fig. 25(a) has an m^2 dependence (m is the barycentric mass of the pions) given by Eq. (11) with $\Delta^2 \to m^2$.

At least ρ exchange must be added to obtain a model of pion-pion scattering. A short-range interaction may be treated approximately by a subtraction adjusted to give the correct $I=0$, $J=0$ scattering length. Such a model would predict an $I=2$ scattering length and an m^2 dependence determined by the behavior of the modified propagator.

ACKNOWLEDGMENTS

I am grateful for the hospitality of the department of Physics and Astronomy at University College, London, where this work was formulated, and to Carolyn Berg of the Laboratory for Nuclear Science computer facility for programming the calculations.

---

*Work supported in part through funds provided by ERDA under No. Contract AT(11-1)-3069.

[1]M. Cini and S. Fubini, Ann. Phys. (N.Y.) 36, 363 (1966).
[2]F. Partovi and E. L. Lomon, Phys. Rev. D 5, 1192 (1972), hereafter referred to as FPL.
[3]Steven Weinberg, Phys. Rev. 177, 2604 (1969).
[4]H. Kim and M. Bander, Phys. Rev. D 4, 265 (1971).
[5]M. Gell-Mann and M. Lévy, Nuovo Cimento 16, 705 (1960).
[6]B. Hyams *et al.*, Nucl. Phys. B64, 134 (1973).
[7]J. L. Basdevant, C. D. Frogatt, and J. L. Petersen, Phys. Lett. 41B, 178 (1972).
[8]M. H. Partovi and E. L. Lomon, Phys. Rev. D 2, 1999 (1970).
[9]E. M. Henley and M. A. Ruderman, Phys. Rev. 92, 1036 (1953); K. M. Watson and J. V. Lepore, *ibid.* 76, 1157 (1949).
[10]A. Klein, Phys. Rev. 90, 1101 (1953).
[11]T. Hamada and I. D. Johnston, Nucl. Phys. 34, 382 (1962).
[12]G. E. Brown and J. W. Durso, Phys. Lett. 35B, 120 (1971).
[13]As indicated in footnote 13 of FPL and after Eq. (4.17) of Ref. 8, we use the mass-shell condition $\vec{p}^2 = \vec{p}'^2 = W^2 - M^2$ rather than $W = M$ in obtaining the energy-independent limit. This guarantees the correct asymptotic behavior and causes the vanishing of terms in Eq. (31) of FPL. The restriction leads to a negligible difference (<1%) in the potential.
[14]R. W. Stagat, F. Riewe, and A. E. S. Green, Phys. Rev. C 3, 552 (1971); R. Bryan and B. L. Scott, Phys. Rev. 177, 1435 (1969).
[15]E. L. Lomon and H. Feshbach, Ann. Phys. (N.Y.) 48, 94 (1968).
[16]M. Lacombe *et al.*, Phys. Rev. D 12, 1495 (1975).
[17]E. L. Lomon, Phys. Rev. D 12, 3758 (1975).